Model Predictive Control Based Dual-Mode Operation of An Energy-Stored Quasi-Z-Source Photovoltaic Power System

Journal:	*Transactions on Industrial Electronics*
Manuscript ID	22-TIE-0524.R1
Manuscript Type:	Regular paper
Manuscript Subject:	Renewable Energy Systems
Keywords:	Energy storage, Model predictive control, Photovoltaic power systems
Are any of authors IEEE Member?:	Yes
Are any of authors IES Member?:	Yes

Model Predictive Control Based Dual-Mode Operation of An Energy-Stored Quasi-Z-Source Photovoltaic Power System

Yushan Liu, *Senior Member*, *IEEE*, Xuyang Liu, Xiao Li, *Member, IEEE*, Haiwen Yuan, Yaosuo Xue, *Senior Member, IEEE*

***Abstract*—The energy-stored quasi-Z-source inverter (ES-qZSI) has attracted much attention for photovoltaic (PV) power generations, due to its capability to stabilize the PV power fluctuations with simple structure and other advantages of Z-source inverter. The improved dual-mode (DM) ES-qZSI is able to support all-weather operation even at night or cloudy days when PV power is extremely low. Whereas, the traditional proportional-integral (PI) based control suffers from complicated controller design and poor dynamic response during mode transition, due to two sets of PI control required for the daytime and night operation modes. In order to overcome that, this paper proposes a model predictive control strategy for the DM-ES-qZSI PV power system. The system predictive models in both day and night operating modes are derived. The control strategy is disclosed to ensure high performance of the system, through calling the predictive models and defined cost functions of the two modes within a single control loop. Simulation and experiment are carried out to verify the effectiveness of proposed control strategy.**

***Index Terms*—Energy storage, Model predictive control, Photovoltaic power systems, quasi-Z-source inverter.**

I. Introduction

THE power of solar cell is intermittent and heavily influenced by the random change of irradiation and temperature. In addition, the power demand on the ac side of the Photovoltaic (PV) power generation system might not be constant. The energy storage technique presents a significant role in PV power systems to store redundant energy or fill up insufficient energy, thus to compensate PV power fluctuations [1]-[3]. The traditional energy storage scheme usually employs an extra DC-DC converter responsible for the charge and discharge management of energy storage battery, which increases the system volume, cost, and control complexity.

The energy-stored quasi-Z-source inverter (ES-qZSI) is able to balance the powers between PV panels and loads, through paralleling the battery to the quasi-Z-source (qZS) capacitors. No additional power converters are required, the system topology and circuit are simplified, and even the cost and reliability are improved, in addition to the characteristics of Z-source inverter [4]-[6]. References [7] and [8] discussed its power flow and put forward a corresponding battery management strategy. References [9] and [10] discussed its working principle, and proposed a control scheme to maintain the power balance among PV panels, energy storage batteries, and loads. Reference [11] contributed to another ES-qZSI by paralleling a battery to capacitor C_1, with three typical operating modes. Another control strategy to maintain constant dc bus peak voltage was proposed in [12]. The modeling and power balancing management of ES-qZSI applying to cascade multilevel system were discussed in [13] and [14]. Considering that the traditional ES-qZSI cannot operate at night or much low PV power conditions, reference [15] modified the topology and resulted into a dual-mode ES-qZSI (DM-ES-qZSI) with day and night modes, which was able to operate in day and night conditions. It was extended to multilevel system in [16].

The DM-ES-qZSI works similar to the traditional ES-qZSI when PV power is sufficient in daytime mode. It also has a night mode, in which the PV panel is cut off from the system, and the battery becomes the only power source to supply the load. The operating principle and control goals are different in the two modes. As a result, two separate sets of proportional-integral (PI) based control strategies were developed for daytime and night operating modes, respectively [15], [16]. Whereas, the ES-qZSI has a coupled impedance network, and one of the qZS capacitor voltages is clamped to the battery voltage. It is usually necessary to coordinate multiple control variables, such as the PV panel voltage and current, qZS inductor current, battery charge and discharge, and inverter output voltage/current, through multiple PI regulators and even cascaded control structure with outer and inner loops. The controller structure and design become complicated, let alone the two sets of PI for the DM-ES-qZSI. In addition, the PI-based control suffers from unstable voltage and current control and poor dynamic performance during the mode switching between the daytime and night modes.

The fuzzy control [17]-[19] and sliding mode control [20] based nonlinear control algorithms have been investigated on the traditional ES-qZSI to improve dynamic response. The former two methods suffer from complicated controller design

Manuscript received February 06, 2021. This work was supported in part by the National Natural Science Foundation of China under Grant 52107175, in part by the Beijing Nova Program under grant Z211100002121080, and in part by the Fundamental Research Funds for the Central Universities under Grant KG16135701, China.

Y. Liu, X. Liu, X. Li and H. Yuan are with the School of Automation Science and Electrical Engineering, Beihang University, Beijing, 100083, China.

Y. Xue is with the Oak Ridge National Laboratory, Oak Ridge, TN 37831, USA.

and difficult digital realization. The later one has few investigations due to the recently emerged Model Predictive Control (MPC) method [21],[22]. The MPC has attracted much attention in power electronics, because of its advantages of effectiveness in multi-objective optimization, simple structure using one single control loop, easy digital implementation, and fast tracking of reference signals [21]. References [23] and [24] performed the MPC to the four-leg and single-phase qZSIs. The MPC for the qZSI based motor drives were discussed in [25]-[27]. A long-horizon MPC was applied to improve the performance of qZSI in [28]. And [29]-[31] studied on the weighting factors elimination for the MPC of qZSI. In addition, the MPC is attractive in applications of modes switching through calling different predictive models and cost functions, instead of designing two or more sets of PI control loops [32],[33]. Whereas, the MPC has not been developed for the ES-qZSI yet, nor for the DM-ES-qZSI.

In this paper, an MPC based control method is proposed for the DM-ES-qZSI PV power system, including the maximum power point tracking (MPPT) of PV panel, battery charging and discharging, and load power stabilization in the daytime operation mode; and the battery discharging and load power stabilization in the night operation mode. The predictive models are established and cost functions are defined, according to the operating principle and control goals of the two modes, respectively. The control method is realized through calling the predictive models and cost functions within one single control loop. Simulation and experimental results demonstrate fast and accurate response, and smooth mode switching. The organization of the paper is as follows. In Section II, the DM-ES-qZSI PV power system is introduced. In Section III, the system predictive models are established. Section IV details the proposed MPC strategy. Section V demonstrates simulation and experimental results, and Section VI concludes the work.

II. DM-ES-qZSI PV Power System

Fig. 1 shows the configuration of DM-ES-qZSI PV power system [15]. There are: i) the PV panel, with one switch K_1 and one terminal capacitor C_{in}; ii) the energy-stored qZS network, including energy storage battery BT, two inductors L_1 and L_2, two capacitors C_1 and C_2, and one transistor K_2; iii) the six transistors formed three-phase inversion bridges; and iv) the three-phase load. An IGBT/MOSFET based transistor K_2 is used to replace the diode in the qZS network of traditional ES-qZSI, allowing the bidirectional power flow. A relay/contactor-based switch K_1 is able to cut off the PV panel from the system at night or in cloudy or rainy days, so as to meet the load power demand through the energy storage battery.

To simplify the analysis, the equivalent model of open circuit voltage with internal resistance is applied to the PV panel and energy storage battery as

$$V_{ocv} = v_{C2} + i_b R_b \quad (1)$$

$$V_{PV} = v_{PV} + i_{PV} R_{PV} \quad (2)$$

where V_{ocv} and R_b are the open circuit voltage and internal resistance of energy storage battery; i_b and v_{C2} are the current and terminal voltage of the battery; V_{PV} and R_{PV} are the open circuit voltage and internal resistance of PV panel; and i_{PV} and v_{PV} are the current and terminal voltage of PV panel. Especially, there will be the capacitor-C_{in} voltage v_{in}=v_{PV} and the qZS inductor-L_1 current i_{L1}=i_{PV} when K_1 is closed at day time.

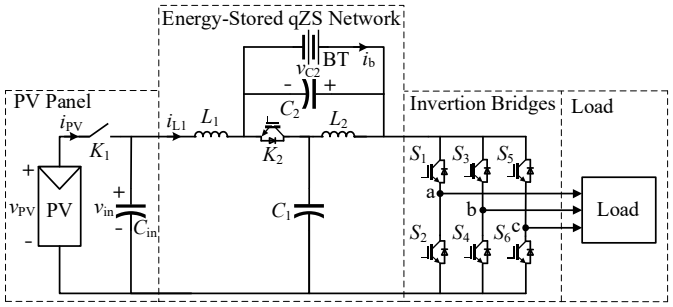

Fig. 1. Topology of dual-mode energy-stored quasi-Z-source photovoltaic inverter system.

III. System Predictive Modeling

From Fig. 1, when the system operates in the daytime with sufficient PV power, the switch K_1 is closed, PV panel is connected to the system and supplies power to the load, while the energy storage battery plays a role in stabilizing the fluctuation of PV power. When operating in insufficient PV power at night, cloudy, or rainy days, the output power of the PV panel is extremely unstable and even unable to output power under extreme conditions. Then the switch K_1 cuts off the PV panel from the system, and the energy storage battery discharges to supply power to the load and maintains the operation of the system. The predictive models of the two operating modes are disclosed as follows, respectively.

A. Predictive Model of qZS Network in Daytime

When the system operates in the daytime, the switch K_1 is closed and the PV panel is connected to the inverter system. The inverter bridges have the non-shoot-through state and shoot-through state as the traditional qZSI, where the upper and lower switches of the same bridge arm can be connected at the same time without damaging the devices during the shoot-through state [5]. The equivalent circuits of the two states are as shown in Fig. 2, in which the three-phase inverter bridge is equivalent to a controlled current source, and the battery current is positive when discharges.

As can be seen from Fig. 2 (a), in the shoot-through time interval T_0, a bridge arm is shoot-through, the switch K_2 turns off, the qZS capacitors discharges, the qZS inductors charges, the DC bus voltage v_{PN} is zero, and the inverter does not contribute power to the load. From Fig. 2 (b), within the non-shoot-through time interval T_1, the switch K_2 obtains the trigger signal and turns on, PV panel charges the qZS capacitors, the qZS inductors release energy, and the load in ac side gains power from the dc side.

According to Kirchhoff current law (KCL) and Kirchhoff voltage law (KVL), the dynamic equations of the system dc side in the shoot-through and non-shoot-through states during daytime operation are obtained as shown in (3) and (4), respectively.

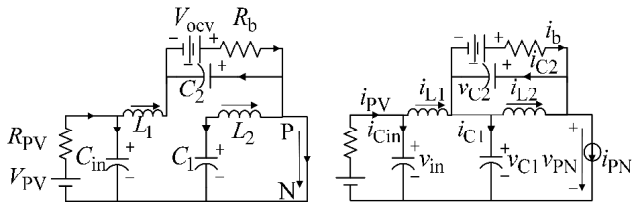

Fig. 2. Equivalent circuit of system dc side during daytime operation. (a) Shoot-through state, and (b) non-shoot-through state.

$$\begin{cases} L_1\dfrac{\mathrm{d}i_{L1}}{\mathrm{d}t}=v_{in}+v_{C2} \\ L_2\dfrac{\mathrm{d}i_{L2}}{\mathrm{d}t}=v_{C1} \\ C_1\dfrac{\mathrm{d}v_{C1}}{\mathrm{d}t}=-i_{L2} \\ C_2\dfrac{\mathrm{d}v_{C2}}{\mathrm{d}t}=-i_{L1}+i_b \\ C_{in}\dfrac{\mathrm{d}v_{in}}{\mathrm{d}t}=i_{pv}-i_{L1} \end{cases} \quad (3) \qquad \begin{cases} L_1\dfrac{\mathrm{d}i_{L1}}{\mathrm{d}t}=v_{in}-v_{C1} \\ L_2\dfrac{\mathrm{d}i_{L2}}{\mathrm{d}t}=-v_{C2} \\ C_1\dfrac{\mathrm{d}v_{C1}}{\mathrm{d}t}=i_{L1}-i_{PN} \\ C_2\dfrac{\mathrm{d}v_{C2}}{\mathrm{d}t}=i_{L2}-i_{PN}+i_b \\ C_{in}\dfrac{\mathrm{d}v_{in}}{\mathrm{d}t}=i_{pv}-i_{L1} \end{cases} \quad (4)$$

From (3), (4), and Fig. 2, the average model of dc side in a switching cycle during daytime operation of the system can be deduced [15]. Then when the system reaches the steady state in the daytime operation, the relationship between the dc-link peak voltage V_{PN}, the average qZS capacitor voltages V_{C1} and V_{C2}, with the average PV panel terminal voltage V_{in} is obtained as

$$\begin{cases} V_{C2}=\dfrac{D}{1-2D}\cdot V_{in} \\ V_{C1}=\dfrac{1-D}{1-2D}\cdot V_{in}=V_{C2}+V_{in} \\ V_{PN}=V_{C1}+V_{C2}=\dfrac{1}{1-2D}\cdot V_{in}=B\cdot V_{in} \end{cases} \quad (5)$$

where $D=T_0/T_s$ is the shoot-through duty ratio, switching cycle T_s includes shoot-through state time interval T_0 and non-shoot-through state time interval T_1.

Forward Euler method is used to discretize equations (3) and (4), and the predictive model of shoot-through and non-shoot-through states during daytime operation are obtained as shown in (6) and (7), respectively.

$$\begin{cases} i_{L1}(k+1)=\left(1-\dfrac{R_{L1}\cdot T_s}{L_1}\right)\cdot i_{L1}(k)+\dfrac{T_s}{L_1}\cdot\left(v_{in}(k)+v_{c2}(k)\right) \\ i_{L2}(k+1)=\left(1-\dfrac{R_{L2}\cdot T_s}{L_2}\right)\cdot i_{L2}(k)+\dfrac{T_s}{L_2}\cdot v_{C1}(k) \\ v_{C1}(k+1)=v_{C1}(k)+R_{C1}\cdot\left(-i_{L2}(k+1)+i_{L2}(k)\right)-\dfrac{T_s}{C_1}\cdot i_{L2}(k) \\ v_{C2}(k+1)=v_{C2}(k)+R_{C2}\cdot\left(-i_{L1}(k+1)+i_{L1}(k)\right)+\dfrac{T_s}{C_2}\cdot\left(i_b(k)-i_{L1}(k)\right) \\ v_{in}(k+1)=v_{in}(k)+R_{Cin}\cdot\left(-i_{L1}(k+1)+i_{L1}(k)\right)+\dfrac{T_s}{C_{in}}\cdot\left(i_{pv}(k)-i_{L1}(k)\right) \end{cases} \quad (6)$$

$$\begin{cases} i_{L1}(k+1)=\left(1-\dfrac{R_{L1}\cdot T_s}{L_1}\right)\cdot i_{L1}(k)+\dfrac{T_s}{L_1}\cdot\left(v_{in}(k)-v_{c1}(k)\right) \\ i_{L2}(k+1)=\left(1-\dfrac{R_{L2}\cdot T_s}{L_2}\right)\cdot i_{L2}(k)+\dfrac{T_s}{L_2}\cdot\left(-v_{c2}(k)\right) \\ v_{C1}(k+1)=v_{C1}(k)+R_{C1}\cdot\left(i_{L1}(k+1)-i_{L1}(k)\right)+\dfrac{T_s}{C_1}\cdot\left(i_{L1}(k)-i_{PN}(k)\right) \\ v_{C2}(k+1)=v_{C2}(k)+R_{C2}\cdot\left(i_{L2}(k+1)-i_{L2}(k)\right)+\dfrac{T_s}{C_2}\cdot\left(i_b(k)+i_{L2}(k)-i_{PN}(k)\right) \\ v_{in}(k+1)=v_{in}(k)+R_{Cin}\cdot\left(-i_{L1}(k+1)+i_{L1}(k)\right)+\dfrac{T_s}{C_{in}}\cdot\left(i_{pv}(k)-i_{L1}(k)\right) \end{cases} \quad (7)$$

B. Predictive Model of qZS Network at Night

When the system operates at night or in the environment with insufficient PV power, the switch K_1 is open, the PV panel is cut off from the system, and the energy storage battery supplies power to the load. Fig. 3 shows the equivalent circuit of the system dc side in night operation.

During night operation, the system still has two states in one switching cycle: i) shoot-through state, during which switch K_2 is off; ii) non-shoot-through state, during which switch K_2 is on. Similarly, the dynamic equations of dc side in the two states can be obtained as shown in (8) and (9), respectively.

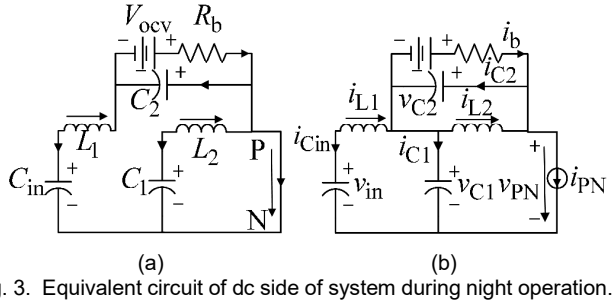

Fig. 3. Equivalent circuit of dc side of system during night operation. (a) Shoot-through state, and (b) non-shoot-through state.

$$\begin{cases} L_1\dfrac{\mathrm{d}i_{L1}}{\mathrm{d}t}=v_{in}+v_{C2} \\ L_2\dfrac{\mathrm{d}i_{L2}}{\mathrm{d}t}=v_{C1} \\ C_1\dfrac{\mathrm{d}v_{C1}}{\mathrm{d}t}=-i_{L2} \\ C_2\dfrac{\mathrm{d}v_{C2}}{\mathrm{d}t}=-i_{L1}+i_b \\ C_{in}\dfrac{\mathrm{d}v_{in}}{\mathrm{d}t}=-i_{L1} \end{cases} \quad (8) \qquad \begin{cases} L_1\dfrac{\mathrm{d}i_{L1}}{\mathrm{d}t}=v_{in}-v_{C1} \\ L_2\dfrac{\mathrm{d}i_{L2}}{\mathrm{d}t}=-v_{C2} \\ C_1\dfrac{\mathrm{d}v_{C1}}{\mathrm{d}t}=i_{L1}-i_{PN} \\ C_2\dfrac{\mathrm{d}v_{C2}}{\mathrm{d}t}=i_{L2}-i_{PN}+i_b \\ C_{in}\dfrac{\mathrm{d}v_{in}}{\mathrm{d}t}=-i_{L1} \end{cases} \quad (9)$$

From (8), (9), and Fig. 3, the average model of dc side in one switching cycle when the system operates at night can be obtained, and the relationship between voltages is shown as

$$\begin{cases} V_{in}=\dfrac{1-2D}{D}\cdot V_{C2} \\ V_{C1}=\dfrac{1-D}{D}\cdot V_{C2}=V_{C2}+V_{in} \\ V_{PN}=V_{C1}+V_{C2}=\dfrac{1}{1-2D}\cdot V_{in}=B\cdot V_{in} \end{cases} \quad (10)$$

Forward Euler method is used to discretize (8) and (9), and the predictive model of shoot-through and non-shoot-through states at night operation mode is deduced as shown in (11) and (12).

$$\begin{cases} i_{L1}(k+1)=\left(1-\frac{R_{L1}\cdot T_s}{L_1}\right)\cdot i_{L1}(k)+\frac{T_s}{L_1}\cdot\left(v_{in}(k)+v_{C2}(k)\right) \\ i_{L2}(k+1)=\left(1-\frac{R_{L2}\cdot T_s}{L_2}\right)\cdot i_{L2}(k)+\frac{T_s}{L_2}\cdot v_{C1}(k) \\ v_{C1}(k+1)=v_{C1}(k)+R_{C1}\cdot\left(-i_{L2}(k+1)+i_{L2}(k)\right)-\frac{T_s}{C_1}\cdot i_{L2}(k) \\ v_{C2}(k+1)=v_{C2}(k)+R_{C2}\cdot\left(-i_{L1}(k+1)+i_{L1}(k)\right)+\frac{T_s}{C_2}\cdot\left(i_b(k)-i_{L1}(k)\right) \\ v_{in}(k+1)=v_{in}(k)+R_{Cin}\cdot\left(-i_{L1}(k+1)+i_{L1}(k)\right)-\frac{T_s}{C_{in}}\cdot i_{L1}(k) \end{cases} \tag{11}$$

$$\begin{cases} i_{L1}(k+1)=\left(1-\frac{R_{L1}\cdot T_s}{L_1}\right)\cdot i_{L1}(k)+\frac{T_s}{L_1}\cdot\left(v_{in}(k)-v_{C1}(k)\right) \\ i_{L2}(k+1)=\left(1-\frac{R_{L2}\cdot T_s}{L_2}\right)\cdot i_{L2}(k)+\frac{T_s}{L_2}\cdot\left(-v_{C2}(k)\right) \\ v_{C1}(k+1)=v_{C1}(k)+R_{C1}\cdot\left(i_{L1}(k+1)-i_{L1}(k)\right)+\frac{T_s}{C_1}\cdot\left(i_{L1}(k)-i_{PN}(k)\right) \\ v_{C2}(k+1)=v_{C2}(k)+R_{C2}\cdot\left(i_{L2}(k+1)-i_{L2}(k)\right)+\frac{T_s}{C_2}\cdot\left(i_b(k)+i_{L2}(k)-i_{PN}(k)\right) \\ v_{in}(k+1)=v_{in}(k)+R_{Cin}\cdot\left(-i_{L1}(k+1)+i_{L1}(k)\right)-\frac{T_s}{C_{in}}\cdot i_{L1}(k) \end{cases} \tag{12}$$

C. Predictive Model of AC Output

An inductive-resistive load with resistance R_L and inductance L_L in series of each phase is applied to the inverter bridge output of Fig. 1. According to Kirchhoff voltage law, the dynamic equation of output current is expressed as

$$\boldsymbol{V}=R_L\boldsymbol{i_o}+L_L\frac{d\boldsymbol{i_o}}{dt} \tag{13}$$

where $\boldsymbol{V}$ and $\boldsymbol{i_o}$ are the vectors of three-phase ac output voltage and current, respectively. From (13), the vector projection formula in two-phase static coordinate system is obtained as

$$\begin{cases} L_L\frac{di_\alpha}{dt}=V_\alpha-R_L\cdot i_\alpha \\ L_L\frac{di_\beta}{dt}=V_\beta-R_L\cdot i_\beta \end{cases} \tag{14}$$

where V_α and V_β are the α and β components of $\boldsymbol{V}$ in two-phase static coordinate system, respectively; i_α and i_β are the α and β components of $\boldsymbol{i_o}$ in two-phase static coordinate system, respectively.

The Forward Euler method is used to discretize (14), and the predictive model of output current in two-phase static coordinate system are obtained as

$$\begin{cases} i_\alpha(k+1)=\left(1-\frac{R_L\cdot T_s}{L_L}\right)\cdot i_\alpha(k)+\frac{T_s}{L_L}\cdot V_\alpha(k) \\ i_\beta(k+1)=\left(1-\frac{R_L\cdot T_s}{L_L}\right)\cdot i_\beta(k)+\frac{T_s}{L_L}\cdot V_\beta(k) \end{cases} \tag{15}$$

Table I lists the eight effective voltage vectors of ac output, including seven $\boldsymbol{V}_1$~$\boldsymbol{V}_7$ for non-shoot-through state and one $\boldsymbol{V}_8$ for shoot-through state. The three-phase qZSI has totally seven ways to obtain the shoot-through state, including shoot through by any one phase leg, combining any two phase legs, and all three phase legs [5]. Whereas, they are redundant because all the seven ways produce the same voltage vector [25]. Therefore, to reduce the calculation, the three phase legs turning on together is applied for the shoot-through state voltage vector.

According to Table I, the eight effective vectors of ac output voltage can be expressed as

$$\boldsymbol{V}_x=\frac{2}{3}\cdot V_{PN}\cdot\left(S_1+a\cdot S_3+a^2\cdot S_5\right) \tag{16}$$

where $x\in[1,\ldots,8]$; V_{PN} is the dc-link peak voltage; $a=e^{j120^\circ}$ is a complex operator; S_1, S_3, and S_5 represent the switching state of upper switches in phases A, B, and C, respectively. The S_n=1 indicates that the switch is on and S_n=0 indicates that the switch is off, $n\in[1,\ldots,6]$.

TABLE I
OUTPUT VOLTAGE VECTORS

states	Voltage vector	S_1	S_2	S_3	S_4	S_5	S_6
Non-shoot-through	$\boldsymbol{V}_1$	1	0	0	1	0	1
	$\boldsymbol{V}_2$	1	0	1	0	0	1
	$\boldsymbol{V}_3$	0	1	1	0	0	1
	$\boldsymbol{V}_4$	0	1	1	0	1	0
	$\boldsymbol{V}_5$	0	1	0	1	1	0
	$\boldsymbol{V}_6$	1	0	0	1	1	0
	$\boldsymbol{V}_7$	1	0	1	0	1	0
Shoot-through	$\boldsymbol{V}_8$	1	1	1	1	1	1

IV. MPC-Based Control Strategy

A. Proposed Control Strategy

When the system is running in the daytime, the PV panel is the main power source to supply power for the whole system, and the energy storage battery is used to compensate PV power fluctuations. The controller needs to ensure: i) PV power tracking maximum power point, ii) stable ac output power, and iii) battery charging and discharging. And the system operates with three ports: PV panel, energy storage battery, and ac load. When two ports are controlled, the third one will automatically match the power difference, and the power balance ignoring the system power loss is:

$$P_{PV}+P_B=P_{out} \tag{17}$$

where P_{PV} is the PV power, which is positive during the day and zero at night; P_B is the power of energy storage battery, which is negative when charging and positive when discharging; P_{out} represents ac load power, constant positive.

When the system operates at night or in the environment with insufficient PV power, the PV panel is cut off from the system. The energy storage battery becomes the only power source to supply power to the load. At this time, the controller needs to ensure: i) stable ac output power, and ii) battery discharging.

When the output power P_{out} is controlled, the energy storage battery power P_B will match automatically.

To achieve the control goals, Fig. 4 shows block diagram of proposed MPC for the DM-ES-qZSI PV power system. The instantaneous circuit variables are measured in the kth sampling period, including dc-side capacitor-C_{in} voltage v_{in}, qZS inductor-L_1 current i_{L1}, and qZS capacitor C_1 and C_2 voltages v_{C1} and v_{C2}, as well as ac-side three-phase load currents i_{abc} transformed to $i_{\alpha\beta}$ in two-phase static frame. Then, based on the established predictive model in daytime and night operation modes, respectively, the state variables $i_{L1}(k+1)$, $v_{in}(k+1)$, and $i_{\alpha\beta}(k+1)$ are predicted for the $(k+1)$th time instant. And through delay compensation, the $i_{L1}(k+2)$, $v_{in}(k+2)$, and $i_{\alpha\beta}(k+2)$ are obtained for the $(k+2)$th time instant. With the reference values of capacitor-C_{in} voltage v_{inref}, qZS inductor-L_1 current i_{L1ref}, and load currents $i_{\alpha ref}$ and $i_{\beta ref}$, the predictions are utilized to compute the control objectives combined cost function. By evaluating the value of cost function at all the eight voltage vectors, the optimal voltage vector, making the minimum cost function, is selected and generates the switching signals S_1~S_6 for the inverter bridges. Once V_8 is selected at shoot-through state, there will be K_2=0; otherwise, K_2=1 in all the other voltage vectors at non-shoot-through state. The switch K_1 is PV power controlled. When the PV power is larger than a threshold $P_{th\text{-}K1}$ in daytime, the controller sends a signal to close the K_1, i.e., K_1=1; otherwise, a signal is sent to open the K_1, i.e., K_1=0, at night operation.

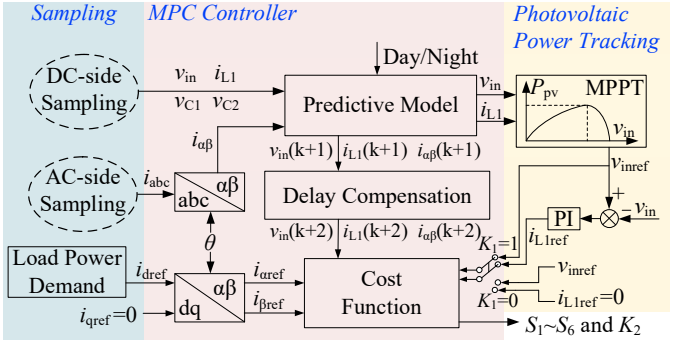

Fig. 4. Block diagram of proposed MPC method for DM-ES-qZSI PV power system.

In addition, the references are determined as follows: i) During daytime operation, the system measures the capacitor-C_{in} voltage v_{in} and qZS current i_{L1} in real time. The improved Perturb and Observe (P&O) based MPPT algorithm obtains the reference PV panel voltage v_{inref} [15]. Then, the difference from v_{inref} and v_{in} going through a PI regulator generates the reference inductor-L_1 current i_{L1ref}. ii) At night operation, since the qZS capacitor-C_2 voltage is clamped at a certain value by the energy storage battery, the v_{inref} can be determined according to (10), so that the proposed MPC tracks the reference capacitor-C_{in} voltage to stabilize the dc-link peak voltage V_{PN}. The i_{L1ref}=0, due to no current flowing through. iii) The active and reactive reference currents i_{dref} and i_{qref} in dq coordinate system are set according to load power demand, no matter daytime or night operation. Then, the reference currents $i_{\alpha ref}$ and $i_{\beta ref}$ in two-phase stationary frame are obtained by coordinate transformation, so as to control ac side output currents i_α and i_β.

B. Cost Function Definition and Implementation

Considering the delay compensation, predictive model for the $(k+2)$th time interval at daytime operation can be obtained from (6), (7) and (15), as

$$\begin{cases} i_\alpha(k+2)=\left(1-\dfrac{R_L\cdot T_s}{L_L}\right)\cdot i_\alpha(k+1)+\dfrac{T_s}{L_L}\cdot V_\alpha(k+1) \\ i_\beta(k+2)=\left(1-\dfrac{R_L\cdot T_s}{L_L}\right)\cdot i_\beta(k+1)+\dfrac{T_s}{L_L}\cdot V_\beta(k+1) \\ i_{L1\_ST}(k+2)=\left(1-\dfrac{R_{L1}\cdot T_s}{L_1}\right)\cdot i_{L1}(k+1)+\dfrac{T_s}{L_1}\cdot\left(v_{in}(k+1)+v_{C2}(k+1)\right) \\ i_{L1\_NST}(k+2)=\left(1-\dfrac{R_{L1}\cdot T_s}{L_1}\right)\cdot i_{L1}(k+1)+\dfrac{T_s}{L_1}\cdot\left(v_{in}(k+1)-v_{C1}(k+1)\right) \end{cases} \tag{18}$$

That for the $(k+2)$th time interval at the night operation can be obtained from (11), (12), and (15), as

$$\begin{cases} i_\alpha(k+2)=\left(1-\dfrac{R_L\cdot T_s}{L_L}\right)\cdot i_\alpha(k+1)+\dfrac{T_s}{L_L}\cdot V_\alpha(k+1) \\ i_\beta(k+2)=\left(1-\dfrac{R_L\cdot T_s}{L_L}\right)\cdot i_\beta(k+1)+\dfrac{T_s}{L_L}\cdot V_\beta(k+1) \\ i_{L1\_ST}(k+2)=\left(1-\dfrac{R_{L1}\cdot T_s}{L_1}\right)\cdot i_{L1}(k+1)+\dfrac{T_s}{L_1}\cdot\left(v_{in}(k+1)+v_{C2}(k+1)\right) \\ i_{L1\_NST}(k+2)=\left(1-\dfrac{R_{L1}\cdot T_s}{L_1}\right)\cdot i_{L1}(k+1)+\dfrac{T_s}{L_1}\cdot\left(v_{in}(k+1)-v_{C1}(k+1)\right) \\ v_{in\_ST}(k+2)=v_{in}(k+1)+R_{Cin}\cdot\left(i_{L1}(k+1)-i_{L1\_ST}(k+2)\right) \\ \qquad\qquad -\dfrac{T_s}{C_{in}}\cdot i_{L1}(k+1) \\ v_{in\_NST}(k+2)=v_{in}(k+1)+R_{Cin}\cdot\left(i_{L1}(k+1)-i_{L1\_NST}(k+2)\right) \\ \qquad\qquad -\dfrac{T_s}{C_{in}}\cdot i_{L1}(k+1) \end{cases} \tag{19}$$

The amplitude difference is the major concern of qZS inductor-L_1 current i_{L1} and capacitor-C_{in} voltage v_{in} with their references. Then the absolute cost function for judging the shoot-through/non-shoot-through states during daytime and night operation are set as

$$\begin{cases} g_{NST}=k_1\cdot\left|i_{L1ref}(k)-i_{L1\_NST}(k+2)\right| \\ \qquad\quad +k_2\cdot\left|v_{inref}(k)-v_{in\_NST}(k+2)\right| \\ g_{ST}=k_1\cdot\left|i_{L1ref}(k)-i_{L1\_ST}(k+2)\right| \\ \qquad\quad +k_2\cdot\left|v_{inref}(k)-v_{in\_ST}(k+2)\right| \end{cases} \tag{20}$$

where k_1 and k_2 are the weighting coefficients of qZS inductor current and terminal capacitor voltage, respectively. In daytime operation, the weighting coefficients are k_1=1 and k_2=0. And they are k_1=0.015 and k_2=1 at night operation.

To minimize the power tracking difference at a certain load condition, the quadratic cost function of controlling the output current during day and night operation of the system is set as

$$g=\left|i_{\alpha ref}(k)-i_\alpha(k+2)\right|^2+\left|i_{\beta ref}(k)-i_\beta(k+2)\right|^2 \tag{21}$$

Fig. 5 shows the flowchart of the proposed control algorithm implementation. With the references and predictions, the g_{ST} and g_{NST} are computed and compared to determine the shoot-through state, where K_2=0 and x=8. Otherwise, the cost function g is computed at the seven switching states of non-shoot-through state, x={1,…, 7}. The one making the minimum value g_{opt} is selected by defining x. Meanwhile, the K_2=1 in this case. Then the switching state K_2 and the optimal switching state S_{opt}=$S(x)$, formed by [S_1,…, S_6] in Table I, are applied to the power devices.

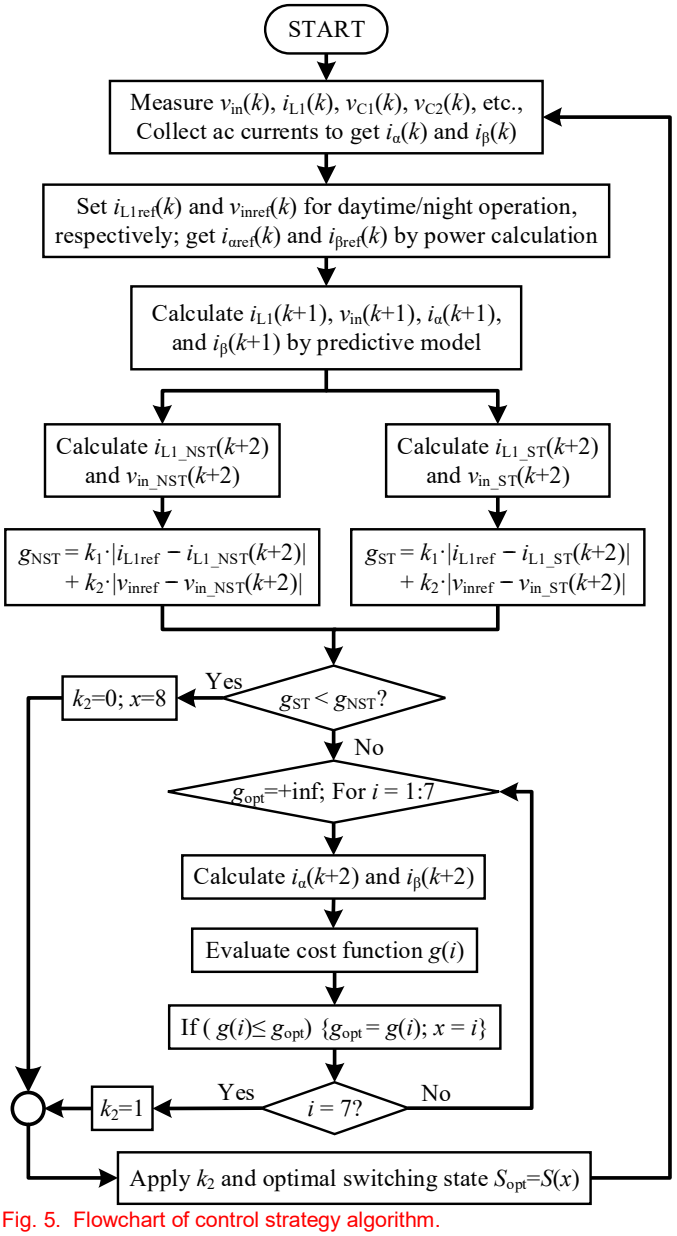

Fig. 5. Flowchart of control strategy algorithm.

V. Simulation and Experimental Investigations

The simulation and experimental tests are carried out on the built DM-ES-qZSI system to verify the proposed control strategy. Table II lists the system parameters. The qZS inductance and capacitance are chosen to limit the switching-frequency ripple of qZS inductor currents within 20%, while that of qZS dc-link peak voltage within 1% [7]. The PV terminal capacitor is designed to buffer the switching-frequency ripple of PV panel voltage within 2% [8]. The 10 mH load inductance is applied according to available laboratory components, which also handles for filtering. Fig. 6 shows the experimental setup. The controller board is based on TMS320F28335 digital signal processor (DSP) to implement the proposed control method. The sampling time is 30 μs. A PV simulator emulates the PV panel characteristics. A bipolar power supply emulates the energy storage battery. A dc contactor is used as K_1. The CM150DY-24A IGBT module is employed for the switch K_2. The three-phase inverter bridge is realized by Intelligent Power Module (IPM) PM50RLA120. A Keysight oscilloscope is utilized to record waveforms.

TABLE II System Specifications

Parameter	Symbols/units	value
PV max. power point voltage	V_{PV}/V	120
PV internal resistance	R_{PV}/Ω	1.0
PV terminal capacitor	C_{in}/μF	100
Battery open circuit voltage	V_{ocv}/V	48
Battery internal resistance	R_{bat}/Ω	1.0
Load resistance	R_L/Ω	10.0
Load inductance	L_L/mH	10.0
qZS inductance	L_1, L_2/μH	600
qZS capacitance	C_1, C_2/μF	470

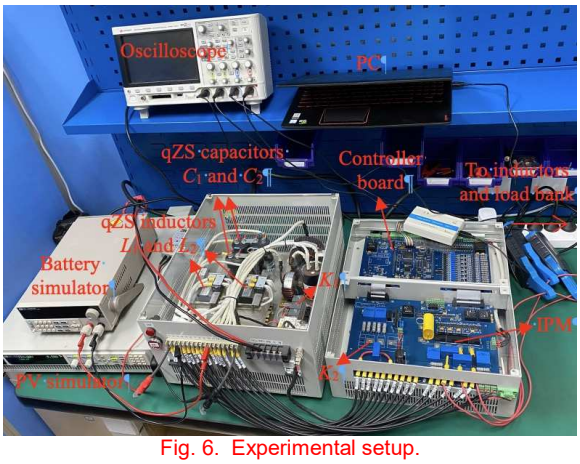

Fig. 6. Experimental setup.

A. Photovoltaic Characteristics Fluctuation in Daytime

The sudden change of PV panel characteristics is firstly investigated to verify the performance of the DM-ES-qZSI PV system using the proposed MPC. The system operates in daytime, the K_1 is closed, and the power demand of the load maintains at 500W. In simulation, the PV panel works at 900W/m^2 and 30℃ in the beginning, which is 600W maximum power point (MPP) power from the PV panel characteristics of 120V MPP voltage and 5.5A MPP current in standard test conditions (STC). At 0.2s, it changes to 600W/m^2 and 27℃, corresponding to 400W MPP power. Similar change is applied in the experiment through regulating the PV emulator. If ignoring the system power loss, the battery power should suddenly change from charging 100W to discharging 100W, to stabilize the fluctuation of PV power. Figs. 7 and 8 show simulation and experimental results, respectively.

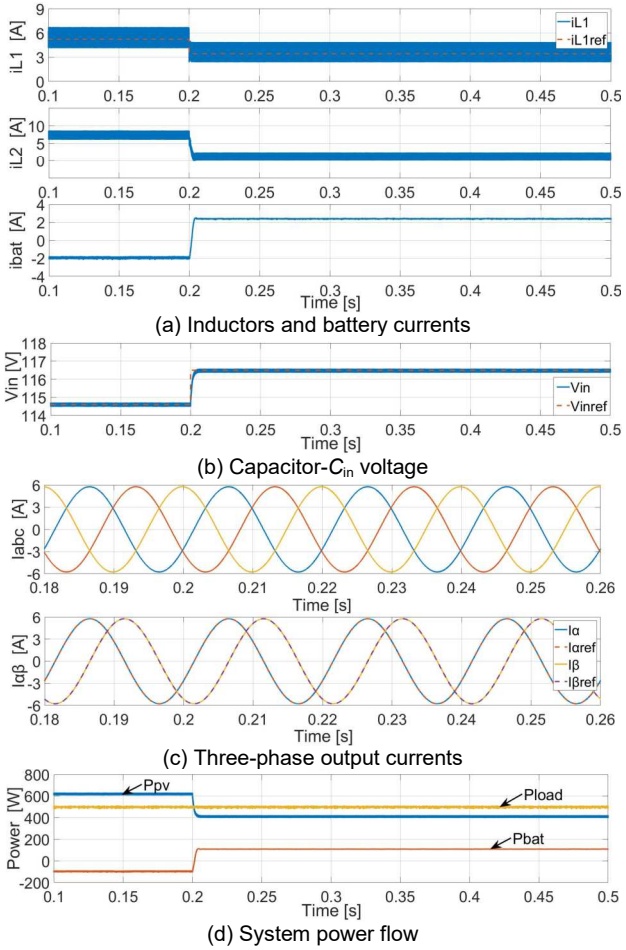

(a) Inductors and battery currents

(b) Capacitor-C_{in} voltage

(c) Three-phase output currents

(d) System power flow

Fig. 7. Simulation results of photovoltaic characteristics fluctuation.

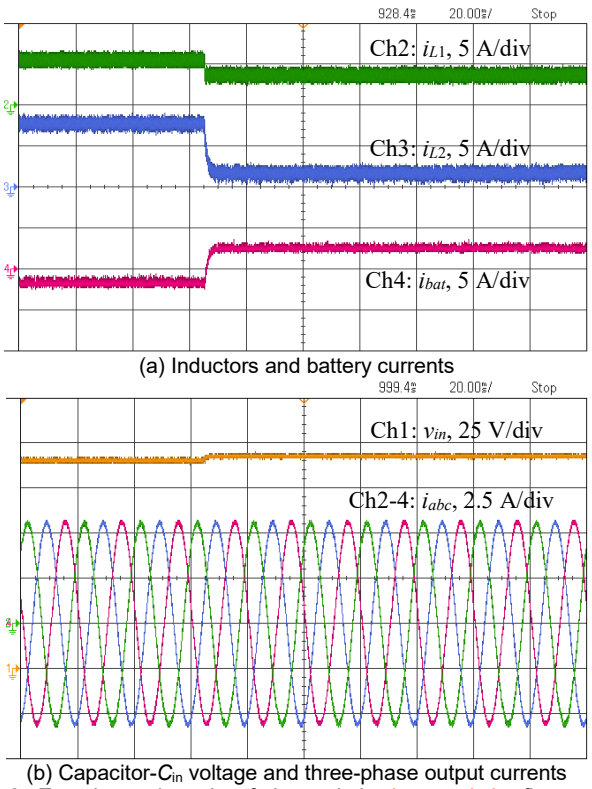

(a) Inductors and battery currents

(b) Capacitor-C_{in} voltage and three-phase output currents

Fig. 8. Experimental results of photovoltaic characteristics fluctuation.

Figs. 7(a) and 8(a) show the current results of L_1, L_2, and battery when the PV characteristics change. It can be seen that the i_{L1} tracks the reference i_{L1ref} accurately in steady state and rapidly during the step change. The battery becomes discharging from 0.2s with fast response. The capacitor-C_{in} voltage v_{in} tracks MPP voltage v_{inref} in Figs. 7 (b) and 8 (b), demonstrating the achieved MPPT. The three-phase output currents i_{abc} in Figs. 7 (c) and 8 (b) are less affected by the fluctuation of PV panel characteristics, which ensures that the load power remains constant. Fig. 7 (d) shows the system power flow in the dynamic process. It can be seen that the PV power, load power, and battery power meet the control goals, and ensures the rapid and stable regulation of the system power flow.

B. Load Power Fluctuation at Night

Sudden change of load power during night operation is investigated, in order to verify the performance of the system operating at night or few PV power conditions. The K_1 is open, and the battery supplies power to the load. The load power demand increases from 350W to 500W. Figs. 9 and 10 show simulation and experimental results, respectively.

From Figs. 9(a) and 10(a), the inductor-L_1 current i_{L1} is zero and the battery current is always positive to discharge in this case. The discharge current increases when the load power changes at 0.2s. In Figs. 9(c) and 10(b), it can be seen that the three-phase output currents i_{abc} are continuously regulated during the transition process. From i_{L1} in Figs. 9 (a) and 10(a), and v_{in} in Figs. 9(b) and 10(b), it can be seen that the controller well controls the two variables and ensures the stability of the system in fast dynamic and accurate steady-state responses. The simulation and experimental results demonstrate that the system has good dynamic performance when the load power changes in the night operation mode.

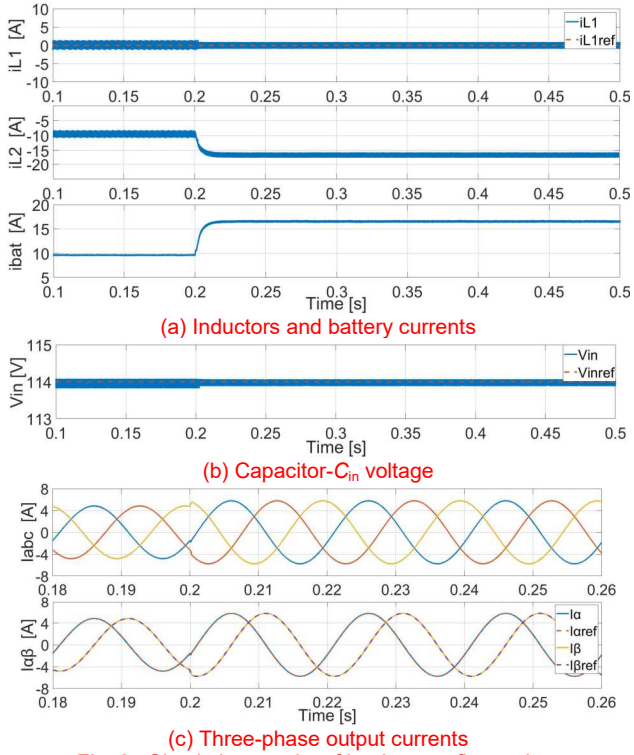

(a) Inductors and battery currents

(b) Capacitor-C_{in} voltage

(c) Three-phase output currents

Fig. 9. Simulation results of load power fluctuation.

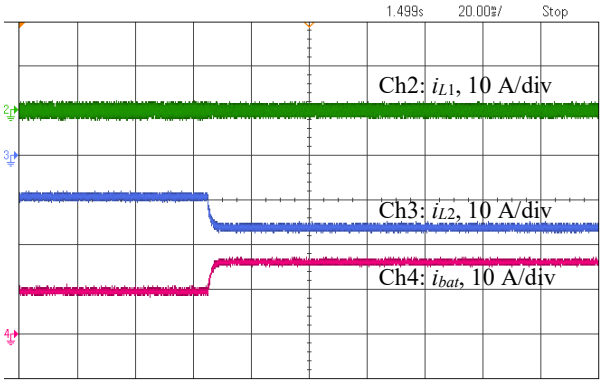

(a) Inductors and battery currents

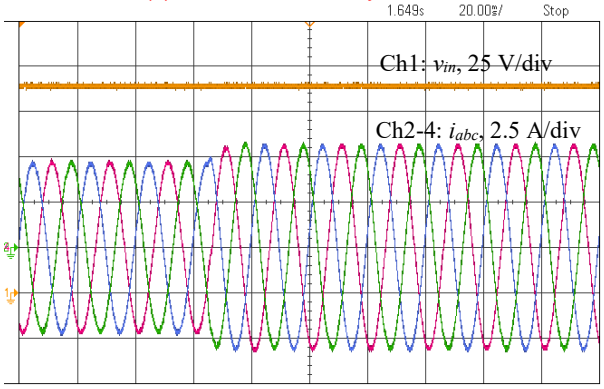

(b) Capacitor-C_{in} voltage and three-phase output currents

Fig. 10. Experimental results of load power fluctuation.

C. Day and Night Operation Mode Switching

Figs. 11 and 12 show the simulation and experimental results during transition between daytime operation and night operation. In simulation, the system operates in the daytime during 0.1~0.2s and 0.4~0.5s. The PV panel with 900W/m^2 and 30℃ is used as the main power source to supply the ac load and charge the battery to store the additional power. During 0.2~0.4s, the system works in the night operation, the PV panel is cut off without any irradiance; only the battery provides power for the ac load. Fig. 12 shows the tested results of mode switching from daytime to night operation.

From Figs. 11(a) and 12(a), it can be seen that the qZS inductor-L_1 current follows its reference accurately in the steady state and fast in the mode switching. The battery current is consistently regulated during the transition process, without significant overshoot or distortion. From Fig. 11 (d), it can be seen that the battery power well compensates the PV power, besides a fast regulation within one fundamental period during the operating mode transition.

From Figs. 11(b) and 12(b), the capacitor-C_{in} voltage v_{in} tracks the MPP voltage during daytime mode, while fast and smooth tracking is achieved during the transition between the two modes. The 500W power is consistently supplied to the load no matter daytime mode or night mode, which can be seen from the unchanged load currents in Figs. 11 (c) and 12 (b).

In addition, the steady-state operation of the system meets the design requirements, and the mode switching process is fast without high overshoot or disturbance, achieving the smooth switching between the dual modes, when using the proposed control strategy.

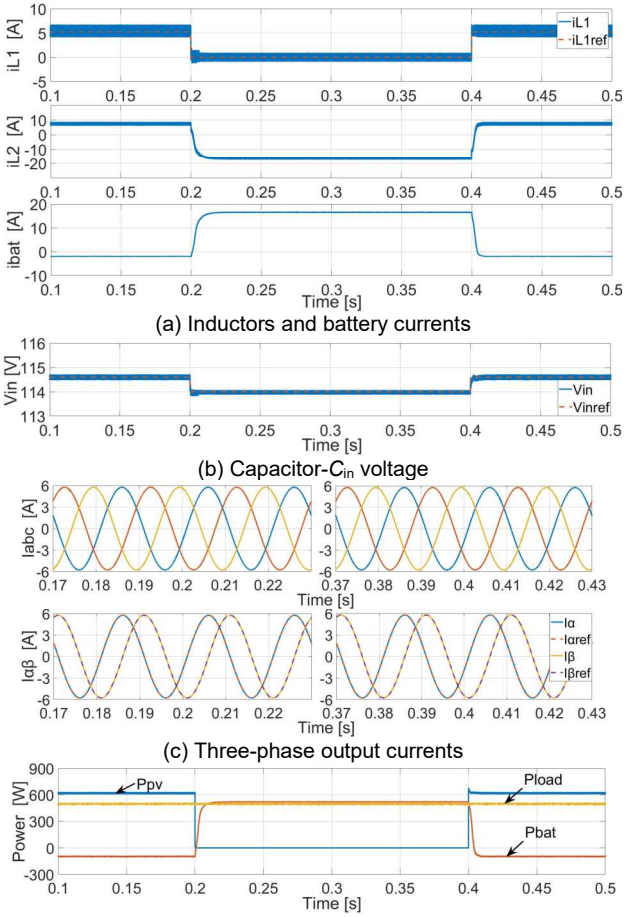

(a) Inductors and battery currents

(b) Capacitor-C_{in} voltage

(c) Three-phase output currents

(d) System power flow

Fig. 11. Simulation results of mode switching.

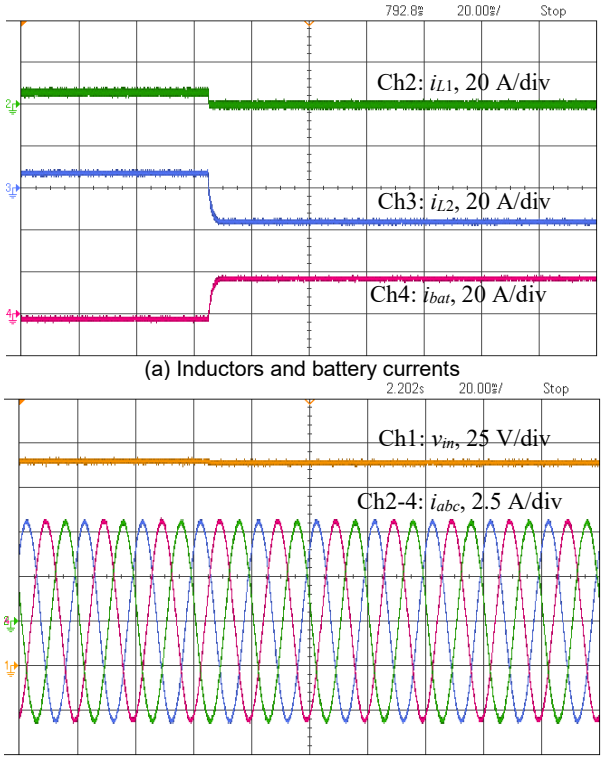

(a) Inductors and battery currents

(b) Capacitor-C_{in} voltage and three-phase output currents

Fig. 12. Experimental results of mode switching.

D. MPPT Investigations

In addition, the MPPT performance is investigated for the DM-ES-qZSI PV power system, with 0.05s refreshing of the MPPT algorithm. The irradiance of PV panel increases from 550W/m^2 to 850W/m^2 and 25℃ at 0.4s. Fig. 13 shows results of the inductor-L_1 current i_{L1} with reference i_{L1ref}, capacitor-C_{in} voltage v_{in} with reference v_{inref}, and powers of three ports. It can be seen that the v_{in} tracks v_{inref} in a fast speed and reaches MPP through several cycles of MPPT time horizon. The i_{L1} keeps following the i_{L1ref} obtained from the outer capacitor voltage control loop. The energy storage battery well compensates the insufficient PV power and stores extra PV power when the PV panel works at MPP.

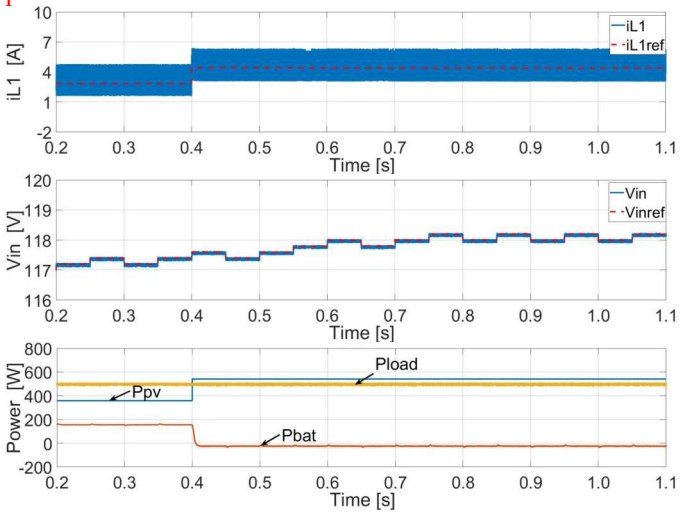

Fig. 13. The inductor-L_1 current i_{L1}, capacitor-C_{in} voltage v_{in}, and powers of three ports when PV characteristics change from 550 to 850 W/m^2.

E. Parameters Dependence

The peak-to-peak ripple of dc-link peak voltage is investigated on passive parameters variations, with the proposed MPC for DM-ES-qZSI PV power system. The ripple ratios are observed when the qZS inductance L, qZS capacitance C, and PV panel terminal capacitance C_{in} vary in the circuit, while all the parameters maintaining unchanged in the controller. The PV panel operates at the STC, and the 500W power is provided to the load through the PV panel and the battery in all cases.

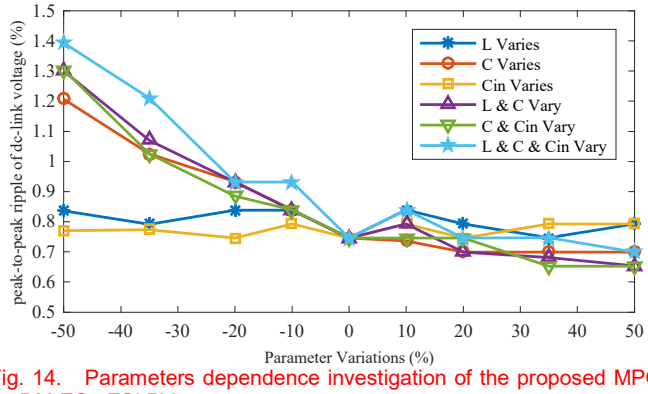

Fig. 14. Parameters dependence investigation of the proposed MPC for DM-ES-qZSI PV power system.

From Fig. 14, it can be seen that the variations of qZS inductance L and PV panel terminal capacitance C_{in} have little effects on the dc-link voltage ripple, while that of qZS capacitance are dominant. In addition, the ripple ratio is still within 1.5% even when all the L, C, and C_{in} changes between ± 50% of nominal values. That demonstrates the low sensitivity to variations in inductors and capacitors values of proposed method.

VI. Conclusion

An MPC strategy was proposed for the DM-ES-qZSI PV power system, in order to enhance the performance for day and night operation. The operating principle of DM-ES-qZSI was analyzed, and the system predictive models were established coordinating different characteristics of the two modes. The control targets were determined, and the control strategy based on MPC was disclosed through a single control loop. Finally, simulation and experimental tests were carried out on PV panel characteristics fluctuation in daytime, load power fluctuation at night, and mode switching between the two modes. The MPPT algorithm and parameters dependence were also investigated. The results demonstrated that the control strategy was simple to achieve multivariable cooperative control, and the system had fast dynamic responses, accurate tracking, and low sensitivity to parameter variations, as well as smooth mode transition using the proposed control.

References

[1] A. Vettuparambil, K. Chatterjee and B. G. Fernandes, "A Multiport Converter Interfacing Solar Photovoltaic Modules and Energy Storage With DC Microgrid," *IEEE Trans. Ind. Electron.*, vol. 68, no. 4, pp. 3113-3123, April 2021.

[2] A. Lashab, D. Sera, F. Hahn, L. Juarez Camurca, M. Liserre and J. M. Guerrero, "A Reduced Power Switches Count Multilevel Converter-Based Photovoltaic System With Integrated Energy Storage," *IEEE Trans. Ind. Electron.*, vol. 68, no. 9, pp. 8231-8240, Sept. 2021.

[3] B. R. Ravada, N. R. Tummuru and B. N. L. Ande, "Photovoltaic-Wind and Hybrid Energy Storage Integrated Multisource Converter Configuration-Based Grid-Interactive Microgrid," *IEEE Trans. Ind. Electron.*, vol. 68, no. 5, pp. 4004-4013, May 2021.

[4] S. A. Singh, G. Carli, N. A. Azeez and S. S. Williamson, "Modeling, Design, Control, and Implementation of a Modified Z-Source Integrated PV/Grid/EV DC Charger/Inverter," *IEEE Trans. Ind. Electron.*, vol. 65, no. 6, pp. 5213-5220, June 2018.

[5] Fang Zheng Peng, "Z-source inverter," *IEEE Trans. Ind. Applicat.*, vol. 39, no. 2, pp. 504-510, March-April. 2003.

[6] H. Abu-Rub, A. Iqbal, S. Moin Ahmed, F. Z. Peng, Y. Li and G. Baoming, "Quasi-Z-Source Inverter-Based Photovoltaic Generation System With Maximum Power Tracking Control Using ANFIS," *IEEE Trans. Sustain. Energy*, vol. 4, no. 1, pp. 11-20, Jan. 2013.

[7] J. G. Cintron-Rivera, Y. Li, S. Jiang and F. Z. Peng, "Quasi-Z-Source inverter with energy storage for Photovoltaic power generation systems," *2011 Twenty-Sixth Annual IEEE Applied Power Electronics Conference and Exposition (APEC)*, 2011, pp. 401-406.

[8] D. Sun, B. Ge, W. Liang, H. Abu-Rub and F. Z. Peng, "An Energy Stored Quasi-Z-Source Cascade Multilevel Inverter-Based Photovoltaic Power Generation System," *IEEE Trans. Ind. Electron.*, vol. 62, no. 9, pp. 5458-5467, Sept. 2015.

[9] Y. Liu, B. Ge, H. Abu-Rub and F. Z. Peng, "Control System Design of Battery-Assisted Quasi-Z-Source Inverter for Grid-Tie Photovoltaic Power Generation," *IEEE Trans. Sustain. Energy*, vol. 4, no. 4, pp. 994-1001, Oct. 2013.

[10] S. Hu, Z. Liang and X. He, "Research on the Dynamic Characteristics and Regulation Method of the Energy Stored Quasi-Z-Source Inverter System," in *IEEE Transactions on Industrial Electronics*, vol. 67, no. 6, pp. 4590-4599, June 2020.

[11] B. Ge et al., "An Energy-Stored Quasi-Z-Source Inverter for Application to Photovoltaic Power System," *IEEE Trans. Ind. Electron.*, vol. 60, no. 10, pp. 4468-4481, Oct. 2013.

[12] B. Ge, F. Z. Peng, H. Abu-Rub, F. J. T. E. Ferreira and A. T. de Almeida, "Novel Energy Stored Single-Stage Photovoltaic Power System With Constant DC-Link Peak Voltage," *IEEE Trans. Sustain. Energy*, vol. 5, no. 1, pp. 28-36, Jan. 2014.
[13] B. Ge, Y. Liu, H. Abu-Rub and F. Z. Peng, "State-of-Charge Balancing Control for a Battery-Energy-Stored Quasi-Z-Source Cascaded-Multilevel-Inverter-Based Photovoltaic Power System," *IEEE Trans. Ind. Electron.*, vol. 65, no. 3, pp. 2268-2279, March 2018.
[14] W. Liang, Y. Liu, B. Ge, H. Abu-Rub, R. S. Balog and Y. Xue, "Double-Line-Frequency Ripple Model, Analysis, and Impedance Design for Energy-Stored Single-Phase Quasi-Z-Source Photovoltaic System," *IEEE Trans. Ind. Electron.*, vol. 65, no. 4, pp. 3198-3209, April 2018.
[15] W. Liang, Y. Liu, B. Ge, X. Li, F.J. Ferreira, and de Almeida, "Night operation, analysis, and control of single-phase quasi-Z-source photovoltaic power system," *IET Renewable Power Generation*, vol. 13, no. 15, pp.2817-2829, Nov. 2019.
[16] W. Liang, Y. Liu and J. Peng, "A Day and Night Operational Quasi-Z Source Multilevel Grid-Tied PV Power System to Achieve Active and Reactive Power Control," in *IEEE Transactions on Power Electronics*, vol. 36, no. 1, pp. 474-492, Jan. 2021.
[17] B. Hamed and N. A. Qaoud, "Fuzzy Control Design for Quasi-Z-Source Three Phase Inverter," *IEEE 7th Palestinian International Conference on Electrical and Computer Engineering (PICECE)*, 2019, pp. 1-6.
[18] M. Bubalo, M. Bašić, D. Vukadinović and I. Grgić, "Optimized Isolated Operation of a WECS- Powered Microgrid with a Battery-Assisted qZSI," *2020 6th International Conference on Electric Power and Energy Conversion Systems (EPECS)*, Istanbul, Turkey, 2020, pp. 1-6.
[19] L. De Oliveira-Assis, E. P. P. Soares-Ramos, P. García-Triviño, R. Sarrias-Mena, C. A. García-Vázquez and L. M. Fernández-Ramírez, "Fuzzy-based Energy Management System for a MVDC PV Power Plant with Battery Stored Quasi-Z-Source Inverter," *2021 IEEE International Conference on Environment and Electrical Engineering and 2021 IEEE Industrial and Commercial Power Systems Europe (EEEIC / I&CPS Europe)*, Bari, Italy, 2021, pp. 1-5.
[20] J. Liu, S. Jiang, D. Cao and F. Z. Peng, "A Digital Current Control of Quasi-Z-Source Inverter With Battery," *IEEE Trans. Ind. Inform.*, vol. 9, no. 2, pp. 928-937, May. 2013.
[21] J. Rodriguez et al., "Predictive Current Control of a Voltage Source Inverter," *IEEE Trans. Ind. Electron.*, vol. 54, no. 1, pp. 495-503, Feb. 2007.
[22] S. Vazquez, J. Rodriguez, M. Rivera, L. G. Franquelo and M. Norambuena, "Model Predictive Control for Power Converters and Drives: Advances and Trends," *IEEE Trans. Ind. Electron.*, vol. 64, no. 2, pp. 935-947, Feb. 2017.
[23] S. Bayhan, H. Abu-Rub and R. S. Balog, "Model Predictive Control of Quasi-Z-Source Four-Leg Inverter," *IEEE Trans. Ind. Electron.*, vol. 63, no. 7, pp. 4506-4516, July 2016.
[24] R. O. Ramírez *et al*., "Finite-State Model Predictive Control With Integral Action Applied to a Single-Phase Z-Source Inverter," in *IEEE Journal of Emerging and Selected Topics in Power Electronics*, vol. 7, no. 1, pp. 228-239, March 2019.
[25] M. Mosa, R. S. Balog and H. Abu-Rub, "High-Performance Predictive Control of Quasi-Impedance Source Inverter," in IEEE Transactions on Power Electronics, vol. 32, no. 4, pp. 3251-3262, April 2017.
[26] H. Mahmoudi, M. Aleenejad and R. Ahmadi, "Modulated Model Predictive Control for a Z-Source-Based Permanent Magnet Synchronous Motor Drive System," *IEEE Trans. Ind. Electron.*, vol. 65, no. 10, pp. 8307-8319, Oct. 2018.
[27] H. Mahmoudi, M. Aleenejad and R. Ahmadi, "Torque Ripple Minimization for a Permanent Magnet Synchronous Motor Using a Modified Quasi-Z-Source Inverter," in *IEEE Transactions on Power Electronics*, vol. 34, no. 4, pp. 3819-3830, April 2019.
[28] A. Ayad, P. Karamanakos and R. Kennel, "Direct Model Predictive Current Control Strategy of Quasi-Z-Source Inverters," in *IEEE Transactions on Power Electronics*, vol. 32, no. 7, pp. 5786-5801, July 2017.
[29] Y. Liu, H. Abu-Rub, Y. Xue and F. Tao, "A Discrete-Time Average Model-Based Predictive Control for a Quasi-Z-Source Inverter," *IEEE Trans. Ind. Electron.*, vol. 65, no. 8, pp. 6044-6054, Aug. 2018.
[30] X. Duan, L. Kang, H. Zhou and Q. Liu, "Multi-Vector Model Predictive Power Control with Low Computational Burden for Grid-Tied Quasi-Z-Source Inverter Without Weighting Factors," in *IEEE Transactions on Power Electronics*.
[31] A. Bakeer, G. Magdy, A. Chub and D. Vinnikov, "Predictive control based on ranking multi-objective optimization approaches for a quasi-Z source inverter," in *CSEE Journal of Power and Energy Systems*, vol. 7, no. 6, pp. 1152-1160, Nov. 2021.
[32] X. Li, Y. Liu and Y. Xue, "Four-Switch Buck–Boost Converter Based on Model Predictive Control With Smooth Mode Transition Capability," in *IEEE Transactions on Industrial Electronics*, vol. 68, no. 10, pp. 9058-9069, Oct. 2021.
[33] X. Li, H. Zhang, M. B. Shadmand and R. S. Balog, "Model Predictive Control of a Voltage-Source Inverter With Seamless Transition Between Islanded and Grid-Connected Operations," in *IEEE Transactions on Industrial Electronics*, vol. 64, no. 10, pp. 7906-7918, Oct. 2017.

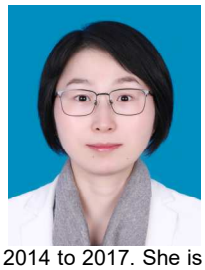

Yushan Liu (S'12–M'15–SM'19) received the B.Sc. degree in automation from Beijing Institute of Technology, Beijing, China, in 2008, and the Ph.D. degree in electrical engineering from the School of Electrical Engineering, Beijing Jiaotong University, Beijing, China, in 2014. She was a Postdoctoral Fellow and an Assistant Research Scientist in the Department of Electrical and Computer Engineering, Texas A&M University at Qatar, Doha, Qatar, from 2014 to 2017. She is currently an Associate Professor in the School of Automation Science and Electrical Engineering, Beihang University, Beijing, China. She has published nearly 100 journal and conference papers, one book, and one book chapter in the area of expertise. Her research interests include power electronics, impedance source inverters, cascade multilevel converters, photovoltaic power integration, and model predictive control, etc.

Dr. Liu received the "Beijing Science and Technology Nova" from Beijing Municipal Science and Technology Commission. She is an Associate Editor of the IEEE TRANSACTIONS ON INDUSTRIAL ELECTRONICS and IEEE OPEN JOURNAL OF INDUSTRIAL ELECTRONICS SOCIETY. She has been the secretary of Power Electronics Devices and Components Committee of IEEE Industry Applications Society since 2022.

Xuyang Liu received the B.Sc. degree in electrical engineering from the School of Automation Science and Electrical Engineering, Beihang University, Beijing, China, in 2021, where he is currently pursuing the M.Sc. degree in electrical engineering.

His research interests include power electronics, impedance source inverters, model predictive control, and wide-bandgap power devices, etc.

Xiao Li (S'14–M'19) received the B.Sc. degree in Automation from Harbin Institute of Technology, China, in 2012, and the Ph.D. degree in Electrical Engineering from Texas A&M University, College Station, TX, USA, in 2017. From 2017 to 2019, he worked with Intersil co., participated in multiple technology programs, including power module design and application of wide-band gap power devices. After that, he joined Efficient Power Conversion Co. (EPC) as a senior application engineer, focusing on application of Gallium Nitride (GaN) power devices into power electronics systems. Since 2021, he has been an Assistant Professor with Beihang University, China. Dr. Li's research interests include modeling and application on wide-bandgap power devices, electronic detection techniques, power electronic techniques in energy systems, etc.

Haiwen Yuan was born in Shanxi, China, in 1968. He received the Ph.D. degree in electrical engineering from Xi'an Jiaotong University, Xi'an, China, in 2003. He is currently a Professor with the School of Automation Science and Electrical Engineering, Beihang University, Beijing, China. His current research interests include electrical and electronics, automatic test and control, and digital signal processing.

Yaosuo Xue (M'03–SM'12) received the B.Sc. degree in electrical engineering from East China Jiaotong University, Nanchang, China in 1991 and the M.Sc. degree in electrical engineering from the University of New Brunswick, Fredericton, Canada, in 2004.

From 1991 to 2000, he was an electrical engineer-in-charge in China Railway Design Corporation and led the traction power systems R&D of the first China's high-speed railway. In 2005-2006, he worked in Capstone Turbine Corporation as a Lead Power Electronics and Systems Engineer. During 2006 to 2008, he was a NSERC PGS-Doctor scholar at the University of New Brunswick. He was with Siemens Corporate Research from 2009 to 2015 and established Corporate Technology USA power electronics program. He is currently with Oak Ridge National Laboratory and his research interests include multilevel converters and smart inverter controls for renewable energy and utility applications.

He is an Associate Editor of the IEEE Transaction on Power Electronics and IEEE Journal of Emerging and Selected Topics in Power Electronics.